Darcy Q. Hou
State Key Laboratory of Hydraulic
Engineering Simulation and Safety, and
School of Computer Science and Technology,
Tianjin University,
Tianjin 300072, China
e-mail: darcy.hou@gmail.com

Arris S. Tijsseling
Department of Mathematics
and Computer Science,
Eindhoven University of Technology,
Eindhoven 5600MB, The Netherlands
e-mail: a.s.tijsseling@tue.nl

Zafer Bozkus
Hydromechanics Laboratory,
Department of Civil Engineering,
Middle East Technical University,
Ankara 06800, Turkey
e-mail: bozkus@metu.edu.tr

Dynamic Force on an Elbow Caused by a Traveling Liquid Slug

The impact force on an elbow induced by traveling isolated liquid slugs in a horizontal pipeline is studied. A literature review reveals that the force on the elbow is mainly due to momentum transfer in changing the fluid flow direction around the elbow. Therefore, to accurately calculate the magnitude and duration of the impact force, the slug arrival velocity at the elbow needs to be well predicted. The hydrodynamic behavior of the slug passing through the elbow needs to be properly modeled too. A combination of 1D and 2D models is used in this paper to analyze this problem. The 1D model is used to predict the slug motion in the horizontal pipeline. With the obtained slug arrival velocity, slug length, and driving air pressure as initial conditions, the 2D Euler equations are solved by the smoothed particle hydrodynamics (SPH) method to analyze the slug dynamics at the elbow. The 2D SPH solution matches experimental data and clearly demonstrates the occurrence of flow separation at the elbow, which is a typical effect of high Reynolds flows. Using the obtained flow contraction coefficient, an improved 1D model with non-linear elbow resistance is proposed and solved by SPH. The 1D SPH results show the best fit with experimental data obtained so far. [DOI: 10.1115/1.4026276]

1 Introduction

For gas-liquid flow in a horizontal pipe different steady flow regimes have been classified [1]. Among these flow regimes the slug flow has been thoroughly investigated because of its violent behavior. Much of the work published on slug flow is related to power plants and oil recovery industries. Dukler and his co-workers proposed theoretical models to predict the development of the slug flow [2], the slug frequency [3], flow regime transition [4,5] and the minimum stable slug length [6]. A review on the modeling of slug flow can be found in Ref. [7]. Pressure surges and impact forces are unavoidable when the liquid slug encounters obstructions such as valves, bends and branches. For a water slug emerging from the end of a horizontal pipe and impacting on a vertical plate, Sakaguchi et al. [8] measured and modeled the generated force. The dynamics of a slug in nearly horizontal pipes [9], a vertical pipe with a bend [10] and an "S" shaped riser [11] was measured and modeled. In these studies, the slug was assumed to be continuous (coherent liquid column of finite length) and steady.

Steady slug flow is less interesting for us. We are interested in a single slug accelerated along a void pipeline by high-pressure gas or steam. The focus is on the hydrodynamic behavior of the slug and its impact on obstructions. The scenario is one where water has accumulated behind a valve in a steam line, and the valve is suddenly opened so that the liquid slug is forced to move along the pipe like a "bullet" in a gun [12]. The slug velocity can easily be over 30 m/s. This scenario frequently occurs and causes trouble in the power industry where electricity is produced by steam turbines. When the slug impacts on an obstruction such as an orifice plate [12] or elbow [13,14], excessive hydrodynamic loads are generated due to its high velocity, which may lead to severe damages. Over 50 incidents have been attributed to this mechanism and an accident was reported in Ref. [15]. Therefore, it is of great

importance to consider this dangerous scenario. Apart from the geometry of the impact target, the most important factor is the impinging slug itself (its velocity, length, and shape) and the driving pressure behind it. As indicated by Bozkus et al. [16], the most needed liquid slug data are those for large diameter pipes used in power-plant piping systems.

A proper understanding of the hydrodynamics of an individual slug traveling in a void line, including its deformation and impact behavior, is important to assess the damage risk and hence take corresponding measures to mitigate it. The objectives of this paper are to review the experimental and mathematical modeling of isolated slug motion and impact, recognize and validate the assumptions in the models, apply the SPH particle method and compare the results with experiments and simulations found in the literature.

The paper is organized as follows. Section 2 reviews previous work on isolated slugs in an initially empty pipeline with an obstruction at its end. In Sec. 3 the 1D model for the motion of the slug before it arrives at the elbow is presented. This model is used to predict the arrival information of the slug at the elbow, such as the slug velocity, slug length, driving air pressure, etc. This information is used as initial condition for the analysis of the slug hydrodynamics at the elbow presented in Sec. 4, at the beginning of which the SPH method is briefly introduced. The general applicability of SPH to engineering problems and associated benefits and shortcomings relative to conventional mesh-based methods are discussed. The Euler equations in SPH disguise governing the slug dynamics at the elbow are presented. Based on the observed 2D flow separation at the elbow, an improved 1D model is then developed. In Sec. 5, the developed models are applied to the experiments of Bozkus [14] and the SPH solutions are compared with numerical results found in the literature. Concluding remarks are given in Sec. 6.

2 State-of-the-Art

Steady slug flow has been intensively studied and the focus was on the kinematic behavior of the slug. However, for a liquid slug in an initially empty line with an obstruction, there is not a wide

range of studies. The first study was probably by Fenton and Griffith [13]. They experimentally and analytically studied the peak forces at an elbow due to clearing a liquid slug initially trapped upstream. Similarly, Neumann [17] studied the forces on a pipe bend resulting from clearing a pool of liquid. After these two attempts, the slug-bend problem gained more attention. Bozkus and his co-authors [14–16,18,19] made great contributions to this topic. Different from Bozkus, Owen and Hussein [12] investigated the hydrodynamic behavior of slugs impacting on an orifice plate. Among these studies, the works of Fenton and Griffith [13], Neumann [17], Bozkus [14], Owen and Hussein [12], and Bozkus et al. [16] need to be underlined due to their original experimental frameworks.

2.1 Laboratory Tests. *Fenton and Griffith* (**1990**). As said, Fenton and Griffith [13] investigated the forces experienced by a pipe bend, when a trapped upstream liquid slug was cleared by a high pressure gas flow. The experimental test rig is shown in Fig. 1. The 2.44 m long pipe with inner diameter of 25 mm was slightly inclined upward and could be filled with water in its lower section, so that liquid slugs with different lengths were obtained. An elbow open to the atmosphere was placed at the end of the pipe. When the ball valve was suddenly opened, the trapped water was forced to move rapidly and hit the elbow. To reduce the effect of structural vibration on the measured impact forces, the elbow was not rigidly fixed to the pipe, but fixed to a support behind it, on which a strain gauge force transducer was installed. Thus, the axial impact forces at the elbow were measured when the slug passed through it. The experiments were varied by changing the initial volume of the entrapped water, the distance of the trapped water to the bend and the driving air pressure in the vessel (414, 552 and 690 kPa). The estimated arrival velocity of the slug at the elbow was varying from 18 to 23 m/s. It was found that the force on the bend was mainly due to quasi-steady momentum transfer in changing the fluid flow direction around the bend. The waterhammer phenomenon was not observed. For slugs that travelled six or more times their initial length, the dispersion was so much that the magnitude of the forces experienced by the bend dramatically dropped.

Neumann (**1991**). Neumann [17] investigated the forces on a pipe bend resulting from clearing a pool of liquid and the effect of different pipe diameters in a setup similar to that of Fenton and Griffith (see Fig. 1). The difference was that the initial trapped water column was replaced by a water pool of varying depth. It was found that the generated forces were insignificant as long as a transition from stratified flow to slug flow did not occur, which was the case when the liquid-air ratio in the pipe was less than 20%. When the transition indeed occurred, it was assumed that, no matter how shallow the pool, the water was concentrated as a slug, the length of which was the water volume divided by the pipe cross-sectional area. The estimated slug impact velocity varied from 17 to 36 m/s. To characterize the slug hydrodynamics, a dimensionless length $D^* = L/L_0$, referred to as dispersion distance,

was used, where L_0 is the initial slug length and L is the distance measured from the tail of the slug to the bend. It was found that for $D^* \approx 5$ the force at the bend was greatly reduced, which is consistent with the findings in Ref. [13]. When $D^* > 6$ the force was negligibly small. When the 1.0 inch pipe connected to the bend (see Fig. 1) was reduced to 0.75 inch, the experimental results did not change much.

Bozkus (**1991**). The experimental setup of Bozkus [14] is depicted in Fig. 2 and consists of a 9.45 m long and 50 mm diameter PVC pipe with a ball valve upstream and a 90 deg elbow downstream. Upstream of the valve there was a pipe section. Its length could be changed to set up water slugs of various lengths. The piping was mounted on seven columns, which in turn were attached rigidly to the concrete floor of the laboratory; in addition, the pipe was rigidly attached to the vessel supplying pressurized air. As a result of the extensive anchoring, the pipe was considered to be rigid and fully constrained from any significant axial motion induced by the slug impact [18]. When the valve was suddenly opened, the slug accelerated due to the pressurized air behind it, hit the elbow and escaped vertically into the atmosphere. Two pressure transducers were installed at the elbow to record the pressure history (see Fig. 2). Slugs with lengths ranging from 1.22 to 3.35 m were propelled into the pipe under air pressures ranging from 69 to 275 kPa.

The peak pressures measured at the elbow varied significantly (largely scattered data) per experimental run, even though nearly identical initial and boundary conditions were imposed. Thus, each test run was repeated 8-10 times. Bozkus attributed the large scattering of the data to the hand-operated valve, because different opening manoeuvres might have affected the slug dynamics. Comparing Figs. 1 and 2, the differences between the two test rigs, such as pipe material, diameter, inclination angle, force measurement, etc., are evident. In addition, the elbow in Fig. 2 was rigidly connected to the pipe.

The estimated arrival velocity of the slug at the elbow varied from 15 to 30 m/s. Consistent measurements were obtained with the two pressure transducers and two general trends were observed. For relatively short slugs ($L_0 = 1.22$ and 1.52 m), the response exhibited a single peak followed by a rapid pressure decay. The effect of air entrainment was so large that the relatively short slugs had practically broken up before reaching the elbow. For relatively long slugs ($L_0 = 2.13$, 2.74 and 3.35 m), a double-peak response was observed. The double-peak phenomenon was correlated to the arrival of two lumps of liquid – instead of one – at the elbow (see Fig. 3), because the single slug had broken up due to a short-lived waterhammer caused by the very rapid valve opening.

Owen and Hussein (**1994**). The test rig of Owen and Hussein [12] is shown in Fig. 4. Upstream of the valve is a pressure source and downstream is an isolated slug of water being propelled into an empty pipe ($D = 50$ mm) and impinging on an orifice with an inner diameter d ranging from 25 to 35.4 mm. Air, with pressures up to 11 bar and of ambient temperature, was used as the driving gas. The volume of the air reservoir was sufficiently large for the
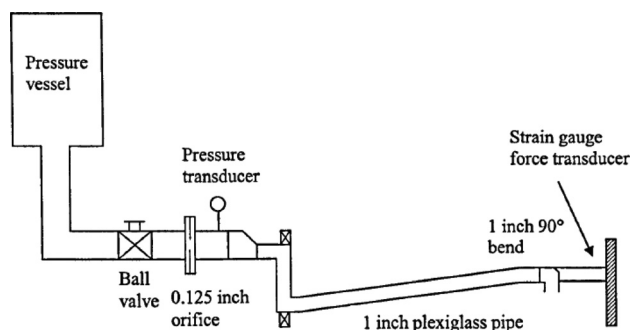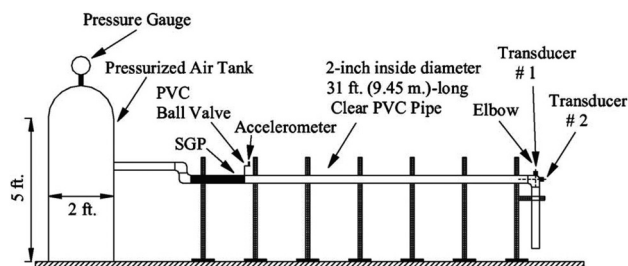

Fig. 1 Experimental setup of Fenton and Griffith [13]

Fig. 2 Experimental setup used by Bozkus in Ref. [14]; SGP = slug generator pipe
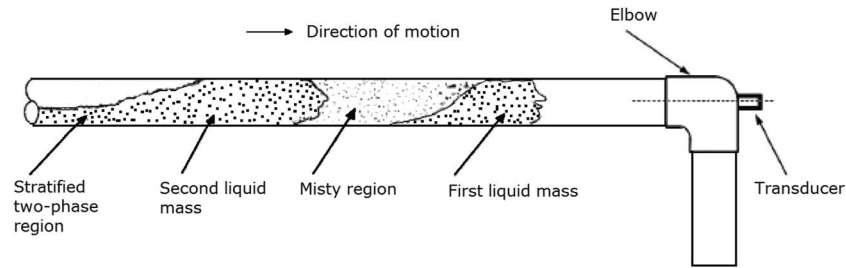
Fig. 3 Flow patterns of the slug motion in a voided line [14]

air pressure drop to be less than 3% in each test. This is different from Bozkus' experiment [14], where a noticeable drop of the driving air pressure occurred. A butterfly valve was located between the reservoir and the steel pipe to enable the rapid air expulsion. The water slug was held between the closed valve and a thin polythene sheet sandwiched between flanges downstream of the valve. By using two different pipes (0.99 and 2.16 m long) to hold the slug, it was possible to obtain three different slug lengths ($L_0 = 0.99$, 2.16 and 3.15 m), while maintaining the overall length of the rig constant at 13.0 m. To measure the slug velocity at the orifice plate, two conductivity probes were situated 0.215 m apart. To measure the impact force at the orifice plate, a pressure transducer was located close to its upstream face. To propel the slug down the pipe, the valve was opened quickly by hand so that the sudden rise in pressure forced the water through the polythene sheet.

Comparing with the test rig of Bozkus [14] (see Fig. 2), the biggest advantage of this experiment is that the velocity of the slug arriving at the impact target (orifice plate) was measured. As shown later, the slug velocity is the most important ingredient in determining the impact force at the target. Another major advantage is the elimination of the manual valve opening effect. In addition, the driving air pressure used in Ref. [12] had a much larger range than that used in Ref. [14].

To confirm the repeatability of the experiment, a number of valve openings were carried out and no significant difference in the slug velocity was detected. This means that no dependence on the hand-operated valve maneuver was observed, whilst Bozkus attributed his largely scattered data to it [14,18]. This suggests that the measurements in Ref. [12] might be more accurate and reliable than those in Ref. [14]. To test whether the orifice plate had an effect on the slug motion towards it, slug velocities with and without the orifice plate were measured. No distinguishable differences between the velocity measurements were observed. This suggests that the air being compressed between the orifice plate and the slug has little effect on the velocity of the slug as it approaches the plate. This is consistent with the conclusion by De Martino et al. [20] that when the orifice ratio d/D (d being the orifice diameter and D is the pipe diameter) is larger than 0.2, the presence of the orifice will not affect the impact velocity of the slug.

For the tests with the 2.16 and 3.15 m long slugs, the traces recorded from the conductivity probes showed a step-change as

Fig. 4 Experimental setup of Owen and Hussein [12]

the front of the slug passed by. For the 0.99 m long slug, however, the recorded trace was extremely erratic, indicating that the slug had broken up. This was confirmed by the trace from the pressure transducer, which showed a much lower impact pressure. This observation is consistent with that in Refs. [13,14,17,18]. The measured arrival velocities were varying from 32 to 58 m/s for the 2.16 m long slug, and from 27 to 42 m/s for the 3.15 m long slug. The measured peak pressures were presented in Ref. [12] but, unfortunately, the pressure traces were absent. This reduces the usefulness of the experimental data for model validation.

Bozkus et al. **(2004).** As indicated by Bozkus and Wiggert [18], the pipe diameter used in Ref. [13] was relatively small compared with the pipe diameters in real piping systems. The weakness of the experimental setup in Ref. [14] was the manual operation of the valve which might have affected the slug dynamics. To avoid these disadvantages, a new experimental setup with the same configuration as that of Fenton and Griffith in Fig. 1 was built. The main differences were that the diameter of the steel pipe was 100 mm instead of 25 mm and that the elbow was rigidly connected to the pipe. As in Ref. [13], the disadvantage was the use of an inclined pipe for slug initialization. The slanted shape of the slug front with respect to the pipe cross-section increases air entrainment in the slug body, especially for short slugs [11,16,21]. Under different driving air pressures (2, 3, 4 and 5 bar), slugs with four initial lengths, $L_0 = 3$, 4, 5, and 6 m, were fired. The arrival velocity of the slug at the elbow was not measured, but the estimated values varied from 15 to 30 m/s. In accordance with $D^* = L/L_0$ being less than 5 for all the slugs (i.e., long slugs), no evident breaking up was observed. Moreover, double-peak phenomena as in Ref. [14] were absent.

2.2 Slug Velocity and Impact Force at the Elbow. When a liquid slug passes through an elbow, dynamic forces will be imparted on it. To predict the force one needs to know the dynamic behavior of the slug, such as the evolution of its pressure and velocity. In Refs. [13,17] the generated axial impact force at the 90 deg elbow is estimated by

$$F = \rho_s A V_{se}^2 \qquad (1)$$

where ρ_s is the liquid slug density, V_{se} is the slug velocity at the elbow and A is the upstream pipe cross-sectional area. Formula (1) is derived from a control volume (CV) around the elbow [22] and has been used to calculate the average pressure (F/A) at a bend [10,11] or on a vertical plate [8]. For steady slug flows, the velocity range is relatively low (0.1–5 m/s [1]), so that the generated impact pressure is small (less than 0.25 bar) and no damage is to be expected [8,10,11]. This is the reason why we stated above that steady slugs are not important for us.

The impact force depends quadratically on the slug arrival velocity at the elbow. For the calculation of the slug velocity different propagation models have been proposed [12–14,16,18]. They are briefly reviewed below. In Refs. [13,17] the slug was assumed to instantaneously accelerate to the "normal
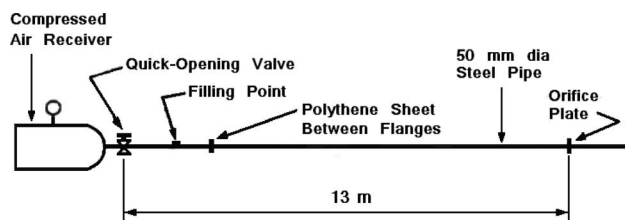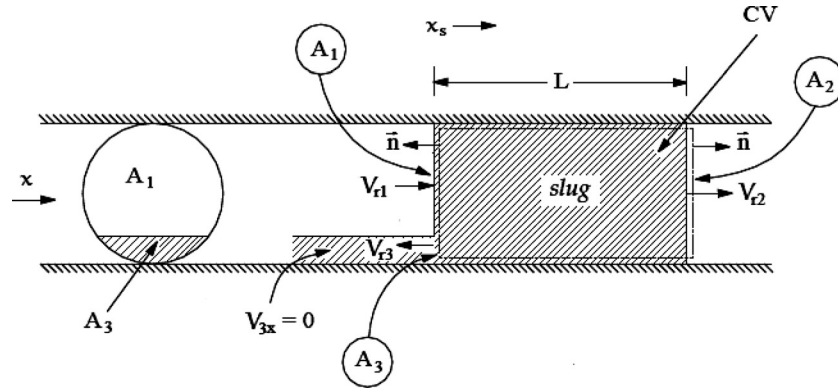
Fig. 5 Control volume moving with the liquid slug in an empty pipe adapted from Ref. [14]; $\beta = A_3/A_2$

velocity" of the driving gas. The force formula (1) underestimated the measured peak force in the worst case by a factor 2.5 for $D^* = L/L_0 < 4$ and largely overestimated it for $D^* > 5$.

The analytical study of Bozkus [14] followed the advanced model in Ref. [13]. The mass loss due to shearing and gravity effects as the slug moves along the pipe was taken into account. For short slugs, the calculated peak pressures were much higher (about 2 times) than the experimental observations. For medium and long slugs, the calculations reasonably matched the experimental peaks, but the trace of the simulated pressure was largely different from the measurements. In Ref. [16], the mass loss from the main slug was neglected and the computed impact pressures underestimated the measured peaks.

A quasi two-dimensional model was developed in Ref. [15], taking air entrainment into account. The water slug was modeled as a number of concentric cylinders sliding through each other. Since the inner cylinders moved faster than the outer ones, air penetrated into the core of the slug tail and the outer liquid cylinders were considered as holdup. At the elbow, the concentric cylinders kept on sliding along each other. This model was applied to the experiment of Bozkus [18] and the experimental peaks were largely underestimated. The predicted pressure traces at the elbow were not in agreement with the measurements. The advantage of the model is that it takes air entrainment into account. The disadvantages concern two aspects. First, since gravity was not considered, the computed flow was symmetric. This is inconsistent with the experimental observation in Ref. [14], which is similar to what is shown in Fig. 5. Second, the effect of the laminar boundary layer was so large that the arrival velocity of the slug at the elbow was dramatically underestimated.

Recently, Kayhan [21] developed a new model in which the holdup coefficient was not constant as in Ref. [14], but a coordinate-dependent function fitted to experimental data. To predict the impact force at the elbow, the effect of the vertical outlet branch was taken into account. Based on many assumptions and complicated 3D coordinate transformations, a 1D numerical approach along a curved line was established. The calculated dynamic forces at the elbow were compared with experiments [14] and numerical calculations of previous researchers [15,18]. The new method predicted the peak pressures with higher accuracy than the previous methods [14,15]. Although the pressure traces also improved, they still largely disagreed with the measurements. The contribution of this new model is that it takes the 3D effect of the elbow flow into account. However, the model is based on a fully developed quasi-steady flow without separation at the elbow, which seems unrealistic.

The model of Owen and Hussein [12] is different from the aforementioned models in many ways. First, instead of numerically solving the gas dynamics equations, the driving air pressure upstream of the slug was directly obtained from a gas expansion formula. Second, the effect of air ahead of the slug was considered, the pressure of which was given by a gas compression formula. Third, the change of the tank pressure was neglected, because the volume of the tank was sufficiently large to prevent a drop in pressure. Fourth, the mass loss (holdup) of the slug during motion was neglected. As stated by Owen and Hussein [12]: "*It was appreciated that as the slug moves through the pipe, it is shedding liquid behind it. However, the area of the slug upon which the gas is acting will still be that of the pipe cross-section, and the total mass of the liquid being accelerated is that of the whole slug.*" The calculated velocities for the 2.16 and 3.15 m slugs (those not breaking up) showed good agreement with the experimental velocities.

3 Slug Dynamics in a Horizontal Line

The mathematical model for slug motion in a horizontal line developed by Bozkus [14] and used in Refs. [16,18,19,21] is briefly revisited. This model is used in this paper to determine the conditions of the slug prior to impact at the elbow.

3.1 Slug Motion in an Empty Pipe. A moving liquid slug that loses mass at its tail is sketched in Fig. 5. In developing the model the following assumptions were made [14]:

The 1D slug is incompressible and has a planar vertical front.

The rigid pipe is fixed in space, hence fluid-structure interaction (FSI) is negligible.

The pressure ahead of the liquid front is atmospheric.

Gas (air) entrainment into the liquid (water) does not occur, (i.e., no mixture).

The shear resistance is assumed to be that of a quasi-steady flow.

The moving slug loses its mass at a constant rate due to shearing and gravity effects. The mass loss is referred to as "holdup" in steady slug flows [2,4–6] and is accounted for in the equations by a holdup coefficient denoted by β ($0 \leq \beta \leq 0.05$).

Applying the Reynolds transport theorem to the moving and shortening control volume shown in Fig. 5, the following governing equations were derived in Ref. [14]:

$$\frac{dV_s}{dt} + \left(\frac{f_s}{2D} - \frac{2}{L}\frac{\beta}{1-\beta}\right)V_s^2 = \frac{P_{\text{tail}} - P_{\text{front}}}{\rho_s L} \qquad (2)$$

$$\frac{dL}{dt} = -\frac{\beta}{1-\beta}V_s \qquad (3)$$

where $\beta = A_3/A_2$ is the holdup coefficient, f_s is the Darcy-Weisbach friction factor, P_{tail} is the air pressure driving the slug (gauge), $P_{\text{front}} = 0$ (gauge), $V_s =$ front velocity, and $(1 - \beta)x_s$

$= \int_0^t V_s dt$ is the position of the advancing slug tail (see Fig. 5). Integrating Eq. (3) gives the following dimensionless formula:

$$\frac{L_{se}}{L_0} = 1 - \frac{\beta}{1 - 3\beta + \beta^2} \frac{L_{\text{pipe}}}{L_0} \qquad (4)$$

which predicts the slug length L_{se} when it arrives at the elbow, and L_{pipe} is the distance from the slug front at its initial position to the elbow. When $\beta \ll 1$, we can further get $L_{se} \approx L_0 - \beta L_{\text{pipe}}$. For β a fixed value as in Ref. [18] or a functional value (depending on the instantaneous slug length) as in Refs. [19,23] can be used. The use of a functional holdup coefficient may result in a more accurate solution, but we take $\beta = 5\%$ constant herein. The initial conditions are

$$V_s(0) = 0, \quad L(0) = L_0 \quad \text{and} \quad x_s(0) = 0 \qquad (5)$$

3.2 Driving Air Pressure. For the air pressure driving the slug, P_{tail} in Eq. (2), one can directly take measured values if available and ignore the gas dynamics involved. However, when gas acoustics is considered, the following differential equations for one-dimensional, unsteady, nonuniform flow of an isothermal compressible gas were used in Ref. [14]

$$\frac{\partial P_a}{\partial t} + V_a \frac{\partial P_a}{\partial x} + \rho_a c_a^2 \frac{\partial V_a}{\partial x} = 0 \qquad (6)$$

$$\frac{\partial V_a}{\partial t} + V_a \frac{\partial V_a}{\partial x} + \frac{1}{\rho_a} \frac{\partial P_a}{\partial x} = -f_a \frac{p_{\text{dry}}}{8A} V_a^2 \qquad (7)$$

$$\frac{dP_a}{dt} = c_a^2 \frac{d\rho_a}{dt} \qquad (8)$$

where the subscript "a" stands for air, $c_a = \sqrt{RT}$ is the isothermal speed of sound with R the universal gas constant and T the gas temperature in Kelvin; p_{dry} is the dry (air) perimeter of the cross-section. Take the initial position of the slug tail as the origin of the axial coordinate. The initial conditions are

$$V_a(x,0) = 0, \quad P_a(x,0) = P_{\text{tank}}(t = 0) = P_0, \quad x < 0 \qquad (9)$$

and the boundary conditions are

$$P_a(-L_{\text{tank}}, t) = P_{\text{tank}}(t), \quad P_a(x_s, t) = P_{\text{tail}}(t), \quad V_a(x_s, t) = V_s(t) \qquad (10)$$

where L_{tank} is the distance from the tank to the slug tail at $t = 0$. The method of characteristics (MOC) was applied to solve the above gas dynamics equations [14,18,21]. The boundary conditions at the slug tail couple the gas Eqs. (6)–(8) to the liquid Eqs. (2) and (3). Note that x_s depends on time. The MOC is employed herein as in Ref. [18] to solve the Eqs. (6)–(8).

The 1D model presented in Secs. 3.1 and 3.2 is used to obtain the velocity with which the slug arrives at the elbow. The arrival time t_{se}, slug velocity V_{se}, slug length L_{se}, and driving air pressure P_{taile}, are then used as initial conditions for the analysis of the slug dynamics at the elbow. The model for the slug motion *after* arrival at the elbow is developed in Sec. 4.

4 Slug Dynamics at the Elbow

From the literature on flow separation at bends [24–27], we realized that the assumption made in Refs. [14,16,18] that the leaving slug occupies the full cross-section of the outlet pipe is not entirely realistic. For high Reynolds flow passing a bend, flow separation easily takes place. This has been verified theoretically [24–26], experimentally [24], and numerically [27]. The passing of a liquid slug through an elbow is a three-dimensional flow

which perhaps can be predicted through solving the full Navier-Stokes equations. Such solutions can be quite difficult to obtain because of air entrainment, turbulence and because the separation surface is not known in advance. Therefore, for the sake of simplicity, we emphasize a two-dimensional solution herein to obtain the contraction coefficient representing flow separation, with which the elbow "resistance" can be properly characterized, and such that the dynamic pressure at the elbow can be obtained with a one-dimensional model. The third dimension of course plays a role in the determination of the contraction coefficient, but for now we have neglected its effect.

If the slug velocity is high and the impact duration is short, gravity, and viscosity can be neglected. The impact duration is taken as the time from the slug arriving at the elbow to the instant when the pressure has decreased to tank pressure. The inviscid two-dimensional flow is governed by the Euler equations with an unknown free streamline (free surface starting at the separation point). To solve the governing equations, the SPH method is applied. This method is briefly reviewed below.

4.1 SPH Method. The SPH method is a meshless, Lagrangian, particle approach that uses an approximation technique to calculate field variables like velocity, pressure, position, etc. In SPH the governing partial differential equations (PDEs) for fluid dynamics are directly transformed into ordinary differential equations (ODEs) by constructing their integral forms with a kernel function and its gradient. Unlike traditional mesh-based methods, such as finite difference method, finite volume method and finite element method, the SPH method uses a set of particles without predefined connectivity to represent a continuum system, and thus it is easy to handle problems with complex geometries. It does not suffer from mesh distortion and refinement problems that limit the usage of traditional methods for large deformation problems and hydrodynamic problems with free surfaces and moving boundaries. As a Lagrangian method, SPH naturally tracks material history information due to movement of the particles, and hence the dedicated surface tracking techniques encountered in traditional mesh-based methods are not needed. It is an ideal alternative for attacking fluid dynamics problems with free surfaces. It has the strong ability to incorporate complex physics into the SPH formulations. Due to the irregularity caused by particle movement, the accuracy of SPH is only first order, which is less than the traditional methods. To compensate the truncated kernel support at boundaries, the enforcement of boundary conditions needs special attention. SPH is generally more time consuming than conventional methods and parallel computation techniques are needed when many particles are used.

Since the invention of SPH in 1977, astrophysical gas flows have been one of the early fields of application [28–30]. Today it is used to model the evolution of the universe with the help of high performance computing (HPC). At the beginning of the 1990s, SPH was used to model high velocity impact (HVI) problems of solids [31] and incompressible free-surface flows [32]. Now SPH is used to simulate a vast range of fluid dynamic problems as shown in the recent reviews [33,34]. However, there is not much published work on SPH applied to pipe flows, which are generally treated as 1D problems. For 1D flows, SPH has not much advantage over traditional mesh-based methods. The most studied case is the shock tube [28,29,35]. Lastiwka et al. [36] used SPH for 1D compressible nozzle flows. Recently, it was successfully employed to model rapid pipe filling [27] and water hammer [37]. The SPH simulations of 2D jets impinging on an inclined wall [38,39] have close relationship with the problem considered herein.

4.2 SPH Fluid Dynamics. For mass density ρ, velocity vector $\mathbf{v}$, position vector $\mathbf{r}$, and pressure p, the Euler equations in discrete SPH form read [32,39]

$$\begin{cases} \dfrac{D\rho_i}{Dt} = \sum_j m_j \mathbf{v}_{ij} \cdot \nabla_i W_{ij}, \\[2mm] \dfrac{D\mathbf{v}_i}{Dt} = -\sum_j m_j \left(\dfrac{p_i}{\rho_i^2} + \dfrac{p_j}{\rho_j^2} + \Pi_{ij} \right) \nabla_i W_{ij}, \\[2mm] \dfrac{d\mathbf{r}_i}{dt} = \mathbf{v}_i, \\[2mm] p_i = c_0^2 (\rho_i - \rho_0) \end{cases} \qquad (11)$$

where subscripts i and j denote particle i and its neighbors j, $\mathbf{v}_{ij} := \mathbf{v}_i - \mathbf{v}_j$, $\mathbf{r}_{ij} := \mathbf{r}_i - \mathbf{r}_j$, $W_{ij} := W(\mathbf{r}_{ij}, h)$ is the cubic-spline kernel and $\nabla_i W_{ij}$ is the gradient of the kernel taken with respect to the position of particle i. The smoothing length h is a size scale of the kernel support and determines the degree to which a particle interacts with its neighbors. The term Π_{ij} represents artificial viscosity of the general form

$$\Pi_{ij} = \frac{-\alpha c_0 h}{\bar{\rho}_{ij}(r_{ij}^2 + 0.01h^2)} \min(\mathbf{v}_{ij} \cdot \mathbf{r}_{ij}, 0) \qquad (12)$$

in which α is a constant [32], c_0 is the speed of sound, ρ_0 is a reference density, $r_{ij} := |\mathbf{r}_{ij}|$ and $\bar{\rho}_{ij} := (\rho_i + \rho_j)/2$. The term Π_{ij} produces a shear and a bulk viscosity to suppress numerical oscillations at sharp wave fronts. The constant α is problem dependent. Its range for problems with shocks is $0.5 \leq \alpha \leq 1$ [28,29,35] and $0.01 \leq \alpha \leq 0.3$ for free-surface flows [32,38]. As shown by Molteni and Colagrossi [38], for free surface flows the SPH solution is not sensitive to the value of α and $\alpha = 0.1$ is commonly used. Here we take $\alpha = 0.1$ as in Ref. [27].

There are four different kinds of boundary conditions for the problem considered herein. The free surface experiences zero pressure and its movement is tracked implicitly in SPH. The image particle method is applied to treat the inflow and outflow boundaries. The mirror particle method is used to impose the free-slip wall boundary condition (see Sec. 3.4.8 in Ref. [39] for details). The Euler forward method is used in Eq. (11) for time marching. The temporal and spatial discretization are dynamically linked to satisfy stability constraints related to the speed of sound and the convective velocity of the flow [39]. Starting from an initial particle distribution ($\mathbf{r}_i$), with given masses m_i (remaining constant), densities ρ_i, pressures p_i, and velocities $\mathbf{v}_i$, each particle marches in time according to Eq. (11).

4.3 1D Fluid Dynamics With Flow Separation. In analogy with the 2D SPH solution, the 1D slug movement *after* impacting the elbow is obtained herein by solving the 1D case of Eq. (11) with constant density and liquid elasticity, which in effect are waterhammer equations in SPH form as used in rapid pipe filling [40]. The upstream boundary condition is calculated from the gas dynamics model described in Sec. 3.2 or directly obtained from experimental gas pressure measurements. To include the effect of flow separation, a new downstream boundary condition has to be derived, for which the control volume sketched in Fig. 6 is utilized.

Applying the unsteady Bernoulli equation between inlet 1 and outlet 2, we have

$$P_{e1} + \frac{\rho_s V_{se1}^2}{2} = P_{e2} + \frac{\rho_s V_{se2}^2}{2} + K_e \frac{\rho_s V_{se1}^2}{2} + \rho_s L_e \frac{dV_{se1}}{dt} \qquad (13)$$

where K_e is the coefficient of minor loss at the elbow, which for steady flow varies from 0.7 to 0.9 [22,41], and L_e is a length scale representing the elbow arc between sections 1 and 2. The last term is an estimate of the inertia involved. To satisfy mass conservation, the outlet flow velocity is
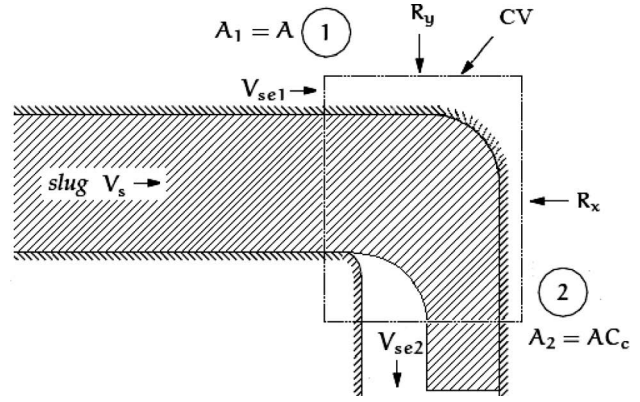

Fig. 6 Control volume for the liquid slug after impact at the elbow and considering flow separation

$$V_{se2} = V_{se1}/C_c \qquad (14)$$

where C_c is the contraction coefficient due to flow separation. With $P_{e2} = 0$ at the open end, and neglecting the inertia term in Eq. (13), one obtains

$$P_{e1} = (1/C_c^2 - 1 + K_e) \frac{\rho_s V_{se1}^2}{2} \qquad (15)$$

This is the nonlinear downstream boundary condition (at cross section 1 upstream of the bend in Fig. 6) for the SPH waterhammer equations modeling (1D) the moving liquid slug. Alternatively, in the rigid-column model, i.e., Eq. (2), P_{front} is replaced by P_{e1} when the slug reaches the elbow. This is in contrast with previous 1D models where $P_{\text{front}} = 0$ all the time. To include possible acoustic effects, the elastic model governed by waterhammer equations is preferred and used herein. The term $1/C_c^2$ is the largest term in Eq. (15), because K_e will be close to zero for a quasi-steady contracting flow.

4.4 Reaction Force and Impulse at Elbow. With $A_1 = A$, $A_2 = AC_c$ and P_{e1} according to Eq. (15), the reaction force in x-direction is

$$R_x = \left(P_{e1} + \rho_s V_{se1}^2 \right) A_1 = \left(\frac{1}{C_c^2} + 1 + K_e \right) \frac{\rho_s V_{se1}^2}{2} A_1 \qquad (16)$$

and with $P_{e2} = 0$ the reaction force in y-direction is

$$R_y = \left(P_{e2} + \rho_s V_{se2}^2 \right) A_2 = \rho_s A_2 V_{se2}^2 = \frac{\rho_s V_{se1}^2}{C_c} A_1 \qquad (17)$$

Based on the obtained pressure history, the axial impulse of the slug at the elbow can be determined by computing the product of the area under the pressure-time curve and the pipe cross-sectional area [13,14], i.e.,

$$I_s = A_1 \int_{t_1}^{t_2} P_e(t) dt. \qquad (18)$$

where $P_e(t)$ is the pressure history at the elbow, and the integral limits t_1 and t_2 are the arrival times at the elbow of the slug front and tail, respectively. To accurately calculate the impulse, not only the peak pressure, but also the duration of the slug impact plays an important role.
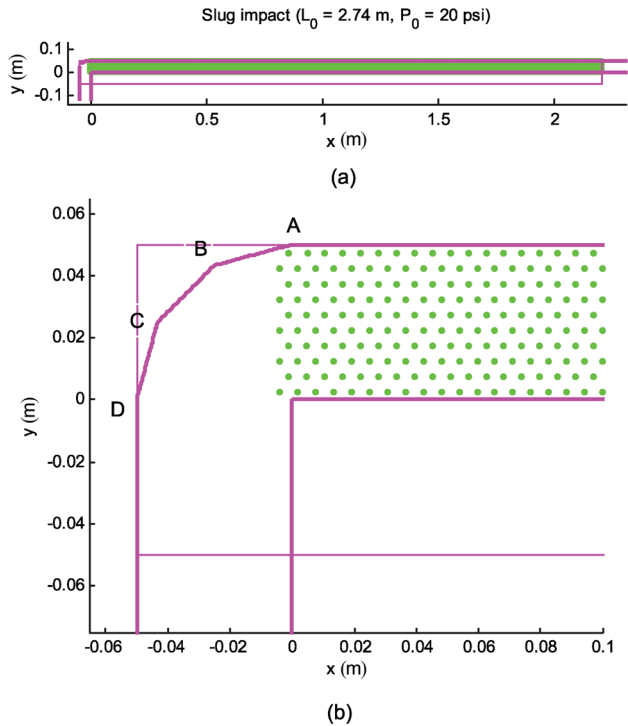
Fig. 7 SPH setup of two-dimensional slug impact at elbow for the case of $L_0 = 2.74$ m and $P_0 = 138$ kPa (20 psig): (a) overview and (b) details at the elbow. The slug moves from right to left toward the elbow with a velocity of $V_{se} = 22.4$ m/s and $L_{se} = 2.2$ m.

Fig. 8 Pressure history after slug impact at the elbow for the case of $L_0 = 2.74$ m and $P_0 = 138$ kPa (20 psig)

5 Results and Discussion

The experiment of Bozkus [14] (see Fig. 2) is simulated in this section. The short slugs are not important for us, because they break up and give relatively small impact forces [12–14,17]. We focus on the medium and long slugs. The speed of sound in the liquid is $c_0 = 440$ m/s, which was determined from spectral analysis of the pressure history recorded by the transducer installed at the SGP (slug generator pipe, see Fig. 2) [14]. The slug density is $\rho_s = 1000$ kg/m^3, $f_s = 0.02$, and $f_a = 0.003$ as in Ref. [18].

5.1 2D SPH Simulations. The 2D SPH setup for the case of $L_0 = 2.74$ m and $P_0 = P_{\text{tank}}(0) = 138$ kPa (20 psi, gauge) is shown in Fig. 7(a). The curved outer wall is modeled by three straight sections as shown in Fig. 7(b). The initial particle distribution is hexahedral (see Fig. 7(b)) with particle spacing $d_0 = 0.0058$ m and the smoothing length is $h = 1.33d_0$. The time step is $\Delta t = 0.2d_0/c_0$. The simulation is stopped when all particles have left the computational domain. There is no viscosity and no holdup at the slug tail ($\beta = 0$). The upstream boundary condition is the measured pressure at the slug arrival time [14] and remains constant. The initial slug velocity is 22.4 m/s and its length reduced to $L_{se} = 2.2$ m according to Eq. (4).

The pressure history of the slug impact at point C is shown in Fig. 8. The calculated arrival time at the elbow has been shifted to that of the experiment (the same holds for the 1D solutions). The 2D SPH solution has a similar trend as the experiment, but suffers from "pressure noise". The pressure noise or spurious oscillation (also seen in other 2D simulations) is due to a numerical artifact, which is a notorious drawback of SPH that has drawn wide attention. After numerical smoothing, the trend of the pressure is comparable with that of the experiment. The fully automated "smooth" scheme, a smoothing procedure for uniformly sampled datasets (see Ref. [42] for the details), has been used. The lower measured pressure magnitude may be attributed to the 3D circular elbow (Fig. 3 herein) instead of the modeled 2D rectangular miter
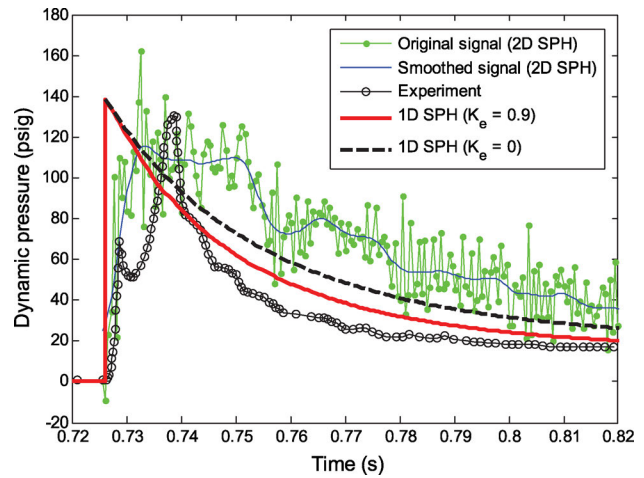
bend (see Fig. 7(b)), the unmodeled slanted water front, the neglected holdup, and the disregarded turbulence. As the difference with the 3D experiment is less than ten percent, these unmodeled physical features are relatively unimportant and can be ignored for the sake of simplicity.

Flow fields at two early times are shown in Fig. 9. Indeed, quasi-steady flow separation has been established after only 0.015 s. That is about one seventh of the duration of the slug impact. This confirms that the 1D model with flow separation developed in Sec. 4.3 is a step in the right direction. The contraction coefficient C_c obtained from the 2D SPH simulations is 0.51, which is close to the theoretical value of 0.5255 for steady flow around a rectangular 2D miter bend [24].

5.2 1D SPH Simulations. In the 1D SPH (elastic) model, the downstream boundary condition is given by Eq. (15) with flow contraction coefficient $C_c = 0.51$ and head loss coefficient $K_e = 0.9$. Again the upstream boundary condition is the measured pressure at the slug arrival time [14], which is held constant. In the numerical setup, the initial particle spacing is $d_0 = 0.01$ m, the smoothing length is $h = 1.2d_0$ and the time step is $\Delta t = d_0/c_0$. The simulation is terminated when all fluid particles are expelled out of the 9.45 m long pipe. For an initial slug length $L_0 = 2.74$ m and initial tank pressure $P_0 = 138$ kPa (20 psig), the estimated pressure at location C (P_{e1} in Eq. (15), with $K_{e=0}$) averaged over all particles in the weakly compressible 1D slug, is shown in Fig. 10, together with numerical solutions from other models. The improved 1D solution is also presented in Fig. 8 for comparison with the 2D solution. Although the double-peak behavior, which is an experimental artefact (see below for details), is not captured, the maximum pressure is well predicted. The simulated trend has good agreement with the measurements 0.015 s after slug arrival when the separated flow is quasi-steady. The difference in the initial 0.015 s is mainly due to the complex flow behavior (two lumps and water-air mixture) at the slug front [14], see Fig. 3. The overall trend predicted in Refs. [14,15,18] contradicted the experimental observations. In Fig. 8 the 1D SPH solution without the head loss ($K_e = 0$) is also shown. The peaks are the same because K_e comes into effect after slug arrival at the elbow. Positive K_e values only reduce the velocity of the slug. For clarity, the 1D pressures shown in Fig. 8 are equal to $(1/C_c^2 - 1)\rho_s V_{se1}^2/2$. The overall trend shifts upward to some extent (when $K_e = 0$) and has better agreement with the inviscid 2D SPH solution.

In the simulations of Bozkus [14,16,18], the velocity V_{se} before and after impact is calculated under the assumption $P_{\text{front}} = 0$ (gauge) and the pressure at the elbow is estimated by
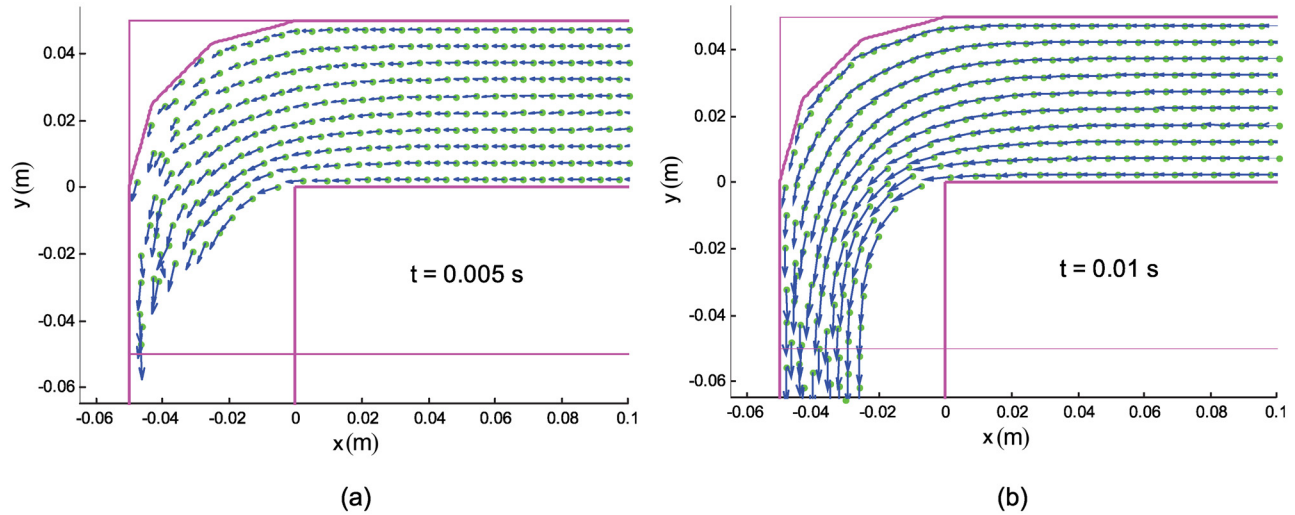
Fig. 9 Flow separation at the elbow at two different times

$$P_e = P_a + \rho_s V_{se}^2 \qquad (19)$$

where P_a is the driving pressure on the back face (tail) of the slug. The slug velocity V_{se} after impact is calculated without considering flow separation and head loss. Then, under driving air pressure and with decreasing mass, the slug passes the elbow with temporal acceleration and hence increasing velocity. This is inconsistent with the decreasing pressure that was measured. In the present model after impact, pressure $P_{\text{front}} = P_{e1}$ given by Eq. (15) acts as a nonlinear "resistance" that reduces the slug velocity and hence the dynamic force and pressure.

Before going further to other cases, let us have a look at the double peak phenomenon observed in the experiments of Bozkus [14]. Those double peaks should not have occurred in the

Fig. 10 Pressure history at the elbow. Comparison between experiments [14] (solid line with circles) and numerical predictions by Bozkus and Wiggert [18] (solid line with squares), Yang and Wiggert [15] (solid line with diamonds) and present 1D SPH (solid line)

first place. As pointed out by Bozkus himself in Ref. [16]: "*The experimental setup of Bozkus in 1991 had a weakness since the slugs were put into motion by opening a fast acting ball valve located just downstream of the slug. The location of the valve may have affected the slug dynamics to some degree since the valve was opened by hand and it was not exactly in the same manner in each run*". As a result of that, he indicated that for longer slugs, the slug separated into two pieces, moving as two slugs in the pipe. Figure 3 shows the flow pattern observed by a camera in the studies of Bozkus [14], subsequent to the slug break-up. The two lumps impinged on the elbow one after another and thus generated the double peaks. He attributed this phenomenon to a short-lived waterhammer taking place across the slug body [14,16,18]. Bozkus also recommended that future experiments be designed using a valve located upstream of the liquid slug to eliminate the valve effect. The main purpose of his new experimental setup in 2004 [16] was to avoid "that human interference" in starting the motion of the slug, and hence the two-peak phenomenon. There were indeed no double peaks in his new but limited experimental results. In addition, double-peak phenomena did not occur in the experiments of Fenton and Griffith [13] and Neumann [17]. In conclusion, the double-peak phenomenon observed for the longer slugs in the experiments of Bozkus [14] is a result of the influence of the ball valve location and the manner in which it was opened.

For a range of slugs with different initial lengths and at different driving air pressures, the 1D SPH results are shown in Fig. 11 together with the measurements [14] and numerical solutions from other researchers [14,15,18,19]. For most of the cases, similar conclusions as drawn above for the case of $L_0 = 2.74$ m and $P_0 = 20$ psig hold. The 1D SPH results with the flow contraction coefficient obtained from 2D SPH simulations agree reasonably well with the experiments. The present model not only predicts the maximum pressure well as shown in Fig. 11 but also gives an accurate prediction of the duration and decreasing trend. As defined by Eq. (18), the impulse is represented by the area under the pressure history curve. Therefore, the numerically predicted impulses by the present model agree very well with the experimental results. The finding in Ref. [13] that the force on the bend is mainly due to quasi-steady momentum transfer in changing the fluid flow direction around the bend is confirmed. The exceptions are mainly for relatively low driving air pressure (10 psig) as shown in Fig. 11(d). It is attributed to the more stratified slug (larger holdup at tail) due to the lower driving pressure and lower
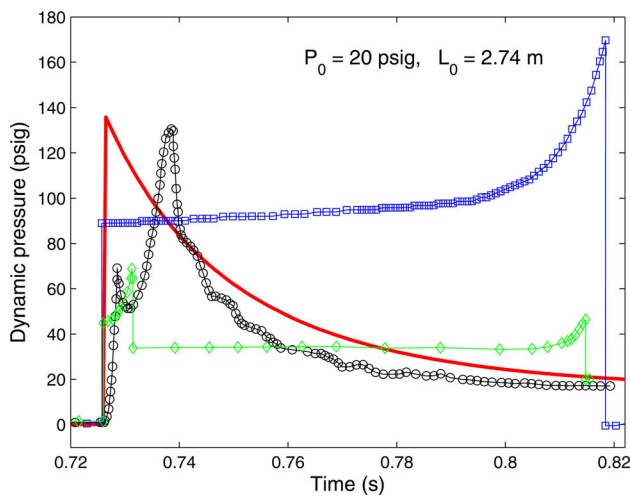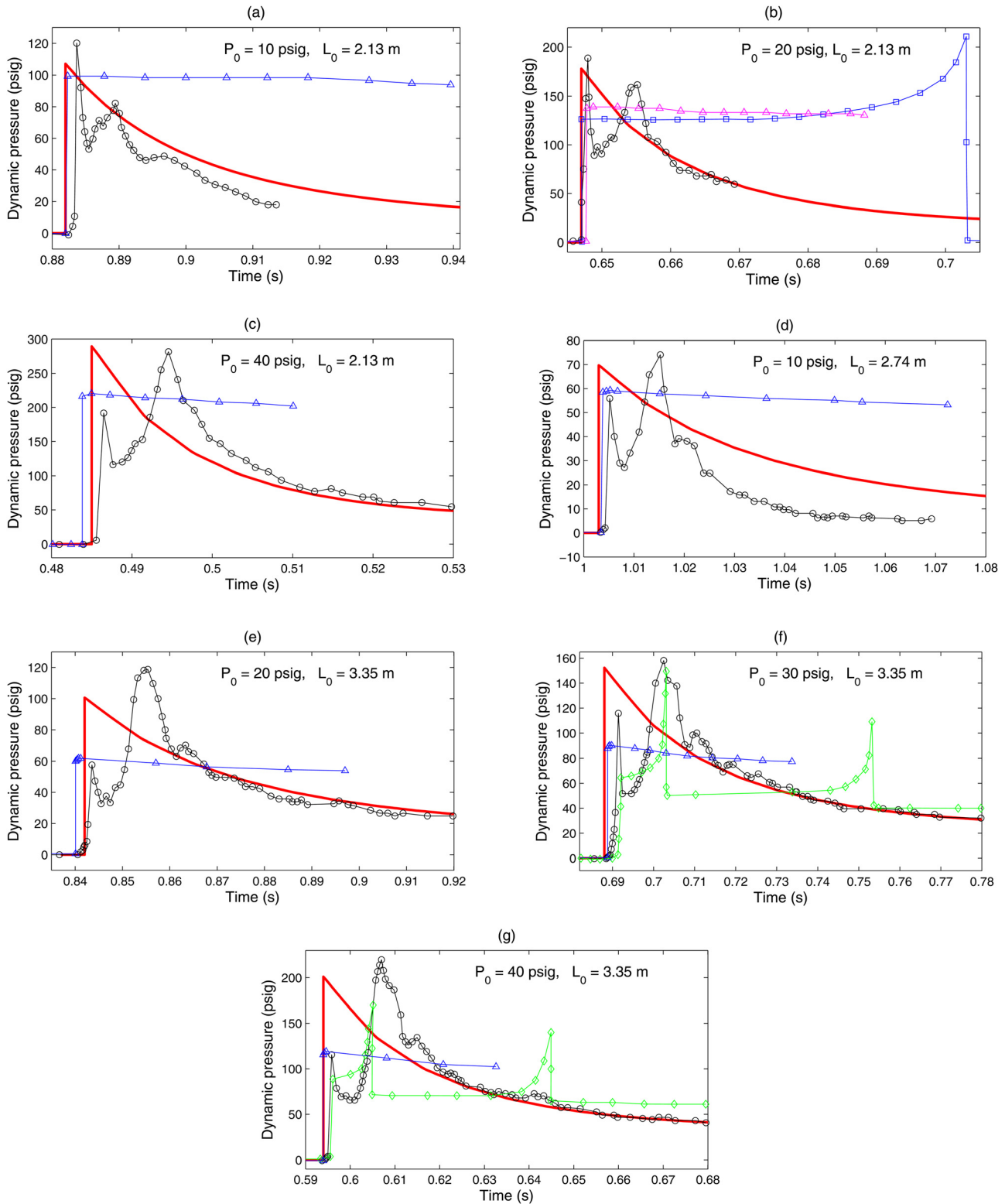
Fig. 11   Pressure history at the elbow. Comparison between experiments [14] (solid line with circles) and numerical predictions by Bozkus and Wiggert [18] (solid line with squares), Yang and Wiggert [15] (solid line with diamonds), Kayhan and Bozkus [19] (solid line with triangles) and present 1D SPH (solid line).

slug velocity. It can also be related to the large data scattering in the experiments (the peak pressures and hence the impulse measured at the elbow varied significantly as mentioned in Ref. [18]). The decreasing pressure trend was predicted in Ref. [19], but the pressure peak magnitude was underestimated to a large extent. The pressure at the end of the impact was largely overestimated too.

6   Conclusions and Recommendations

The dynamic force due to traveling isolated slugs in a horizontal pipeline ending with an open elbow is investigated through 1D and 2D SPH simulations. The generated pressure at the elbow is mainly due to change in flow direction. To accurately predict the

dynamic force, flow separation at the elbow (2D/3D effect) has to be taken into account. With the flow contraction coefficient obtained from a 2D SPH solution, the pressure upstream of the elbow is derived from a control-volume approach and used as the downstream boundary condition in the 1D SPH elastic model. Two essential features of slug impact, i.e., the pressure magnitude and the impact duration, have been well predicted by both the 1D and 2D models. With a properly modeled elbow "resistance" due to flow separation, the improved 1D model is recommended for practical use because it is simple and sufficiently accurate.

Acknowledgment

Nomenclature

A = cross-sectional area (m^2)
c_0 = speed of sound in liquid (m/s)
c_a = speed of sound in air (m/s)
C_c = contraction coefficient
d = diameter of orifice (m)
d_0 = initial particle spacing (m)
D = pipe diameter (m)
D^* = dimensionless dispersion distance
f_a = Darcy-Weisbach friction factor (air)
f_s = Darcy-Weisbach friction factor (water slug)
F = dynamic force (N)
h = smoothing length (m)
i, j = particle index
I_s = axial impulse (N·s)
K_e = minor loss coefficient at elbow
L = distance from slug tail to bend (m)
L_0 = initial slug length (m)
L_e = elbow length (m)
L_{pipe} = distance from slug front to bend (m)
L_{se} = length of slug when arriving at elbow (m)
L_{tank} = pipe length from tank exit to slug tail (m)
m_j = mass of particle j (kg)
p_{dry} = dry perimeter of conduit cross-section (air) (m)
P_a = driving air pressure (psig)
P_e = pressure at elbow (psig)
P_{front} = air pressure at slug front (psig)
P_{tail} = air pressure at slug tail (psig)
P_{taile} = air pressure at slug tail when front arrives at elbow (psig)
P_{tank} = tank pressure (psig)
$\mathbf{r}$ = position (vector) (m)
R = the universal gas constant
R_x = reaction force in x direction (N)
R_y = reaction force in y direction (N)
t = time (s)
t_{se} = arrival time of slug at elbow (s)
T = air temperature (K)
$\mathbf{v}$ = particle velocity (vector) (m/s)
V_a = air velocity (m/s)
V_s = slug velocity (m/s)
V_{se} = velocity of slug when arriving at elbow (m/s)
$W(|\mathbf{r}|, h)$ = kernel function
x_s = position of slug tail (m)
α = constant coefficient in artificial viscosity
β = holdup coefficient
ρ_0 = reference density (kg/m^3)
ρ_a = air density (kg/m^3)
ρ_i = density of particle i (kg/m^3)
ρ_s = liquid slug density (kg/m^3)
Π = artificial viscosity (m^2/s)
FSI = fluid-structure interaction
HPC = high-performance computing
HVI = high-velocity impact
MOC = method of characteristics
ODE = ordinary differential equation
PDE = partial differential equation
SGP = slug generator pipe
SPH = smoothed particle hydrodynamics

References

[1] Mandhane, J. M., Gregory, G. A., and Aziz, K., 1974, "A Flow Pattern Map for Gas-Liquid Flow in Horizontal Pipes," Int. J. Multiphase Flow, **1**(4), pp. 537–553.

[2] Dukler, A. E., and Hubbard, M. G., 1975, "A Model for Gas-Liquid Slug Flow in Horizontal and Near Horizontal Tubes," Ind. Eng. Chem. Fundam., **14**(4), pp. 337–347.

[3] Taitel, Y., and Dukler, A. E., 1977, "A Model for Slug Frequency During Gas-Liquid Flow in Horizontal and Near Horizontal Pipes," Int. J. Multiphase Flow, **3**(6), pp. 585–596.

[4] Taitel, Y., and Dukler, A. E., 1976, "A Model for Predicting Flow Regime Transitions in Horizontal and Near Horizontal Gas-Liquid Flow," AIChE J., **22**(1), pp. 47–55.

[5] Taitel, Y., Barnea, D., and Dukler, A. E., 1980, "Modelling Flow Pattern Transitions for Steady Upward Gas-Liquid Flow in Vertical Tubes," AIChE J., **26**(3), pp. 345–354.

[6] Dukler, A. E., Maron, D. M., and Brauner, N., 1985, "A Physical Model for Predicting the Minimum Stable Slug Length," Chem. Eng. Sci., **40**(8), pp. 1379–1386.

[7] Fabre, J., and Liné, A., 1992, "Modeling of Two-Phase Slug Flow," Annu. Rev. Fluid Mech., **24**, pp. 21–46.

[8] Sakaguchi, T., Ozawa, M., Hamaguchi, H., Nishiwaki, F., and Fujii, E., 1987, "Analysis of the Impact Force by a Transient Slug Flowing out of a Horizontal Pipe," Nucl. Eng. Des., **99**, pp. 63–71.

[9] Zhang, H. Q., Jayawardena, S. S., Redus, C. L., and Brill, J. P., 2000, "Slug Dynamics in Gas-Liquid Pipe Flow," J. Energy Res. Technol., **122**(1), pp. 14–21.

[10] Tay, B. L., and Thorpe, R. B., 2004, "Effects of Liquid Physical Properties on the Forces Acting on a Pipe Bend in Gas-Liquid Slug Flow," Trans. IChemE, Part A, Chem. Eng. Res. Des., **82**(A3), pp. 344–356.

[11] Das, I. A. F., 2003, "The Characteristics and Forces due to Slugs in an "S" Shaped Riser," Ph.D. thesis, Cranfield University, Cranfield, UK.

[12] Owen, I., and Hussein, I. B., 1994, "The Propulsion of an Isolated Slug Through a Pipe and the Forces Produced as it Impacts Upon an Orifice Plate," Int. J. Multiphase Flow, **20**(3), pp. 659–666.

[13] Fenton, R. M., and Griffith, P., 1990, "The Force at a Pipe Bend Due to the Clearing of Water Trapped Upstream," Transient Thermal Hydraulics and Resulting Loads on Vessel and Piping Systems, ASME, PVP190, pp. 59–67.

[14] Bozkus, Z., 1991, "The Hydrodynamics of an Individual Transient Liquid Slug in a Voided Line," Ph.D. thesis, Michigan State University, East Lansing, MI.

[15] Yang, J., and Wiggert, D. C., 1998, "Analysis of Liquid Slug Motion in a Voided Line," ASME J. Pressure Vessel Technol., **120**(1), pp. 74–80.

[16] Bozkus, Z., Baran, Ö. U., and Ger, M., 2004, "Experimental and Numerical Analysis of Transient Liquid Slug Motion in a Voided Line," ASME J. Pressure Vessel Technol., **126**(2), pp. 241–249.

[17] Neumann, A., 1991, "The Forces Exerted on a Pipe Bend due to a Pipe Clearing Transient," M.Sc. thesis, MIT, Cambridge, MA.

[18] Bozkus, Z., and Wiggert, D. C., 1997, "Liquid Slug Motion in a Voided Line," J. Fluids Struct., **11**(8), pp. 947–963.

[19] Kayhan, B. A., and Bozkus, Z., 2011, "A New Method for Prediction of the Transient Force Generated by a Liquid Slug Impact on an Elbow of an Initially Voided Line," ASME J. Pressure Vessel Technol., **133**(2), p. 021701.

[20] De Martino, G., Fontana, N., and Giugni, M., 2008, "Transient Flow Caused by Air Expulsion Through an Orifice," J. Hydraul. Eng., **134**(9), pp. 1395–1399.

[21] Kayhan, B. A., 2009, "Prediction of the Transient Force Subsequent to a Liquid Mass Impact on an Elbow of an Initially Voided Line," Ph.D. thesis, Middle East Technical University, Ankara, Turkey.

[22] Streeter, V. L., Wylie, E. B., and Bedford, K. W., 1998, *Fluid Mechanics*, 9th ed., McGraw-Hill, Boston.

[23] Laanearu, J., Annus, I., Koppel, T., Bergant, A., Vučković, S., Hou, Q., Tijsseling, A. S., Anderson, A., and van't Westende, J. M. C., 2012, "Emptying of Large-Scale Pipeline by Pressurized Air," J. Hydraul. Eng., **138**(12), pp. 1090–1100.

[24] Lichtarowicz, A., and Markland, E., 1963, "Calculation of Potential Flow With Separation in a Right-Angled Elbow With Unequal Branches," J. Fluid Mech., **17**(4), pp. 596–606.

[25] Mankbadi, R. R., and Zaki, S. S., 1986, "Computations of the Contraction Coefficient of Unsymmetrical Bends," AIAA J., **24**(8), pp. 1285–1289.

[26] Chu, S. S., 2003, "Separated Flow in Bends of Arbitrary Turning Angles, Using the Hodograph Method and Kirchhoff's Free Streamline Theory," ASME J. Fluids Eng., **125**(3), pp. 438–442.

[27] Hou, Q., Kruisbrink, A. C. H., Pearce, F. R., Tijsseling, A. S., and Yue, T., "Smoothed Particle Hydrodynamics Simulations of Flow Separation at Bends," Comput. Fluids., **90**, pp. 138–146.

[28] Monaghan, J. J., 1992, "Smoothed Particle Hydrodynamics," Annu. Rev. Astron. Astrophys., **30**, pp. 543–574.

[29] Rosswog, S., 2009, "Astrophysical Smooth Particle Hydrodynamics," New Astron. Rev., **53**(4-6), pp. 78–104.

[30] Springel, V., 2010, "Smoothed Particle Hydrodynamics in Astrophysics," Annu. Rev. Astron. Astrophys., **48**, pp. 391–430.

[31] Libersky, L. D., Petschek, A. G., Carney, T. C., Hipp, J. R., and Allahdadi, F. A., 1993, "High strain Lagrangian hydrodynamics: A three-dimensional SPH code for dynamic material response," J. Comput. Phys., **109**(1), pp. 67–75.

[32] Monaghan, J. J., 1994, "Simulating Free Surface Flows With SPH," J. Comput. Phys., **110**(2), pp. 399–406.

[33] Liu, M. B., and Liu, G. R., 2010, "Smoothed Particle Hydrodynamics (SPH): An Overview and Recent Developments," Arch. Comput. Methods. Eng., **17**(1), pp. 25–76.

[34] Monaghan, J. J., 2012, "Smoothed Particle Hydrodynamics and Its Diverse Applications," Annu. Rev. Fluid Mech., **44**, pp. 323–346.

[35] Price, D. J., 2012, "Smoothed Particle Hydrodynamics and Magneto-hydrodynamics," J. Comput. Phys., **231**(3), pp. 759–794.

[36] Lastiwka, M., Basa, M., and Quinlan, N. J., 2009, "Permeable and Non-Reflecting Boundary Conditions in SPH," Int. J. Numer. Meth. Fluids, **61**(7), pp. 709–724.

[37] Hou, Q., Kruisbrink, A. C. H., Tijsseling, A. S., and Keramat, A., 2012, "Simulating Transient Pipe Flow With Corrective Smoothed Particle Method," Proceedings of 11th International Conference on Pressure Surges, BHR Group, Lisbon, Portugal, pp. 171–188.

[38] Molteni, D., and Colagrossi, A., 2009, "A Simple Procedure to Improve the Pressure Evaluation in Hydrodynamic Context Using the SPH," Comput. Phys. Commun., **180**(6), pp. 861–872.

[39] Hou, Q., 2012, "Simulating Unsteady Conduit Flows With Smoothed Particle Hydrodynamics," Ph.D. thesis, Eindhoven University of Technology, Eindhoven, The Netherlands. Available at:http://repository.tue.nl/733420

[40] Hou, Q., Zhang, L. X., Tijsseling, A. S., and Kruisbrink, A. C. H., 2012, "Rapid Filling of Pipelines With the SPH Particle Method," Procedia Eng., **31**, pp. 38–43.

[41] Crane, 1985, "Flow of Fluids Through Valves, Fittings, and Pipe," Technical Paper 410, Crane Co.

[42] Garcia, D., 2010, "Robust Smoothing of Gridded Data in One and Higher Dimensions With Missing Values," Comput. Stat. Data Anal., **54**(4), pp. 1167–1178.